Superconductivity in a two monolayer thick indium film on Si(111)$\sqrt{3} \times \sqrt{3}$-B

Takahiro Ogino,[1] Insung Seo,[2] Hiroo Tajiri,[3] Masashi Nakatake,[4] Sho-ichi Takakura,[4,5] Yudai Sato,[6] Yukio Hasegawa,[6] Yoshihiro Gohda,[2] Kan Nakatsuji,[2] and Hiroyuki Hirayama[1,*]

[1]*Department of Physics, Tokyo Institute of Technology, J1-3, 4259 Nagatsuda, Midori-ku, Yokohama 226-8502, Japan*
[2]*Department of Materials Science and Engineering, Tokyo Institute of Technology, J1-3, 4259 Nagatsuda, Midori-ku, Yokohama 226-8502, Japan*
[3]*Japan Synchrotron Radiation Research Institute/SPring-8 1-1-1 Kouto, Sayo, Hyogo 679-5198, Japan*
[4]*Aichi Synchrotron Radiation Center, 250-3 Minamiyamaguchi-cho, Seto-shi, Aichi-ken 489-0965, Japan*
[5]*Synchrotron Radiation Research Center, Nagoya University, Furo-cho, Chikusa-ku, Nagoya-shi, Aichi-ken 464-8603, Japan*
[6]*The Institute for Solid State Physics, The University of Tokyo, Kashiwanoha 5-1-5, Kashiwa, Chiba 277-8581, Japan*

(Received 29 March 2022; revised 13 July 2022; accepted 18 July 2022; published 28 July 2022)

Two-monolayer-thick In film with a $\sqrt{7} \times \sqrt{3}$-rect structure is known to show superconductivity at 3.18 K on the Si(111)7×7 substrate. We synthesized the $\sqrt{7} \times \sqrt{3}$-In-rect film on the Si(111)$\sqrt{3} \times \sqrt{3}$-B substrate and found that it also became a superconductor at $T_c = 2.38$ K. The In film on the $\sqrt{3}$-B substrate showed the two-dimensional free-electron-like circular Fermi surface as on the 7 × 7 substrate. However, the butterfly-wing-like shape contour at the Fermi surface was found to be shifted and enlarged on the $\sqrt{3}$-B substrate. Density functional calculations revealed that it was caused by the difference of the substrate. T_c on the $\sqrt{3}$-B substrate was considered to be identical to that on the 7 × 7 substrate in consideration of the recently reported surface defect density dependence of T_c. These results indicated that the interaction with the substrate does not play a crucial role in the superconductivity of the two-monolayer-thick In film.

DOI: 10.1103/PhysRevB.106.045423

I. INTRODUCTION

Recent progress in epitaxial growth opens up a frontier of the superconductivity in one or two atomic layer thick films on semiconductor substrates [1–3]. For an example, two-monolayer (ML) thick $\sqrt{7} \times \sqrt{3}$-In-rect film on a Si(111)7×7 substrate has been reported to show the superconductivity at $T_c = 3.18$ K, which is almost the same as that in bulk (3.4 K) [2]. The atomic arrangement of the $\sqrt{7} \times \sqrt{3}$-In-rect film is very close to that of the (001)-oriented bulk In [4,5]. Thus, the superconductivity of the two-ML-thick $\sqrt{7} \times \sqrt{3}$-In-rect film could be regarded as an ultimate thin limit of the bulk In crystal. However, physical properties of such extremely thin layers are readily modified by the interaction with the substrate interface. Actually, one-ML-thick FeSe film was reported to show superconductivity at a much higher T_c of 109 K [6] than that of 9 K in bulk. The enormous increase in T_c was suggested to be caused by the modification of the electronic states by the interaction at the interface. In these respects, it is of great interest to elucidate whether the superconductivity of the two-ML-thick $\sqrt{7} \times \sqrt{3}$-In-rect film is the intrinsic nature of the film or due to the interaction at the interface. For this purpose, we synthesized the two-ML-thick $\sqrt{7} \times \sqrt{3}$-In-rect film on the unconventional Si(111)$\sqrt{3} \times \sqrt{3}$-B substrate and investigated the effect of the interface on the electronic structure and superconductivity by comparing the results with those on the Si(111)7×7 substrate.

II. METHODS

The Si(111)$\sqrt{3} \times \sqrt{3}$-B substrate was prepared by a thermal treatment of highly B-doped Si(111) samples ($\rho = 0.0015$ Ωcm) in ultrahigh vacuum [7]. The $\sqrt{7} \times \sqrt{3}$-In-rect film was synthesized by the deposition of ca. 10 ML In atoms at room temperature and subsequent annealing at 450 °C for 5 min. The $\sqrt{7} \times \sqrt{3}$-In-rect structure was found to be completed by waiting for one hour after the annealing on the Si(111)$\sqrt{3} \times \sqrt{3}$-B substrate irrespective of the amount of deposition. In atoms desorb easily at the annealing temperature. The insensitivity of the formation of the two-ML-thick $\sqrt{7} \times \sqrt{3}$-In-rect structure to the amount of the deposited In atoms is considered to be due to the instability of In triple layers [4]. However, In atoms migrate readily on the Si(111)$\sqrt{3} \times \sqrt{3}$-B substrate at which all the surface dangling bonds are fully passivated [8,9]. Therefore, it is regarded to be necessary to wait for a long time until the readily migrating In atoms settle to the stable sites to complete the $\sqrt{7} \times \sqrt{3}$-In-rect structure on the Si(111)$\sqrt{3} \times \sqrt{3}$-B substrate.

Successful formation of the two-ML-thick $\sqrt{7} \times \sqrt{3}$-In-rect film on the Si(111)$\sqrt{3} \times \sqrt{3}$-B substrate was confirmed using low-energy electron diffraction (LEED), scanning tunneling microscope (STM), and surface x-ray diffraction (SXRD). SXRD were conducted at the beamline BL13XU [10] in SPring-8. The ultrahigh vacuum apparatus, which enables *in situ* sample preparation, on a S2+D2 type diffractometer was available on the beamline. After an asymmetrically cut Si(111) double-crystal monochromator [11], two mirrors were located for rejecting higher harmonics from

*hirayama.h.aa@m.titech.ac.jp

the in-vacuum undulator. SXRD data were taken with a photon energy of 20 keV at room temperature.

Superconductivity of the $\sqrt{7} \times \sqrt{3}$-In-rect film on the Si(111)$\sqrt{3} \times \sqrt{3}$-B substrate was examined using scanning tunneling spectroscopy (STS) with a W tip at low temperatures. STS spectra were obtained with a lock-in amplifier at a modulation voltage of 0.03 meV at 971 Hz. The feedback loop was kept closed during the spectrum measurements.

Electronic structure of the $\sqrt{7} \times \sqrt{3}$-In-rect film on the Si(111)$\sqrt{3} \times \sqrt{3}$-B substrate was investigated using angle resolved photoelectron spectroscopy (ARPES) and first-principles density functional theoretical (DFT) calculations. ARPES measurements were conducted at room temperature at BL7U in Aichi SR. Details of the DFT calculations will be given later.

III. RESULTS AND DISCUSSION

A. Structure

LEED and STM images of the $\sqrt{7} \times \sqrt{3}$-In film on the Si(111)$\sqrt{3} \times \sqrt{3}$-B substrate are shown in Figs. 1(a) and 1(b), respectively. LEED showed the characteristic (3/5 3/5) fractional order spots of the $\sqrt{7} \times \sqrt{3}$ periodicity from the threefold rotational domains on the Si(111) substrate. The $\sqrt{7} \times \sqrt{3}$-In film on the Si(111)$\sqrt{3} \times \sqrt{3}$-B substrate was observed to include several defects in STM. However, at the area other than the defects, the atomically resolved $\sqrt{7} \times \sqrt{3}$ STM image was observed as shown in the inset.

In atoms were reported to have one-ML-thick $\sqrt{7} \times \sqrt{3}$-In-hex and two-ML-thick $\sqrt{7} \times \sqrt{3}$-In-rect structures on the Si(111)7×7 substrate [12]. The superconductivity was found to emerge only on the two-ML-thick $\sqrt{7} \times \sqrt{3}$-In film on the Si(111)7×7 substrate [4]. Thus, we examined the thickness and the interface structure of the $\sqrt{7} \times \sqrt{3}$-In film on the Si(111)$\sqrt{3} \times \sqrt{3}$-B substrate using SXRD.

First, we confirmed that the $\sqrt{3} \times \sqrt{3}$-B reconstruction was still preserved at the interface even after the synthesis of the $\sqrt{7} \times \sqrt{3}$-In on the Si substrate. For this purpose, we first confirmed that the whole substrate surface was covered by the $\sqrt{7} \times \sqrt{3}$-In film by carefully checking that the substrate-originated $\sqrt{3} \times \sqrt{3}$ diffraction spots disappeared completely and only the $\sqrt{7} \times \sqrt{3}$ diffraction spots were observed on the In samples using reflection high energy electron diffraction (RHEED). Then, we examined the existence of the $\sqrt{3} \times \sqrt{3}$ fractional ordered diffractions at the interface buried under the In film by in-plane SXRD scans. Actually, we detected the diffraction of the (1/3 1/3) fractional ordered rod which originates from the $\sqrt{3} \times \sqrt{3}$ but not from the $\sqrt{7} \times \sqrt{3}$ periodicity. It proved that the B-induced $\sqrt{3} \times \sqrt{3}$ reconstruction was still preserved at the In/Si interface.

Then, we confirmed that the In film has two-ML-thickness by measuring the (00) crystal truncation rod (CTR) profile. The experimentally observed (00) CTR profile is shown by the black dotted curve in Fig. 1(c). The x ray was incident along the [11$\bar{2}$] orientation for the measurement. The CTR profile was fitted by a kinematical simulation code [13] for one- and two-ML-thick $\sqrt{7} \times \sqrt{3}$-In-hex and -rect films on the Si(111) $\sqrt{3} \times \sqrt{3}$-B substrate. The pristine Si(111)$\sqrt{3} \times \sqrt{3}$-B surface reconstruction is formed by the B atoms at the S_5 subsurface site with the $\sqrt{3} \times \sqrt{3}$ periodicity and Si

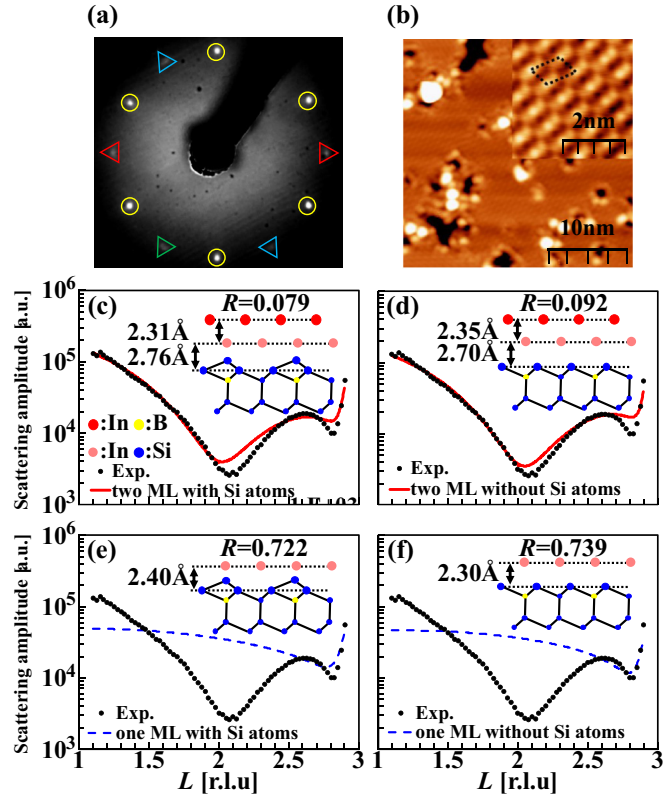

FIG. 1. LEED pattern (a) and STM image (b) of the $\sqrt{7} \times \sqrt{3}$-In phase on the Si(111)$\sqrt{3} \times \sqrt{3}$-B substrate. The characteristic (3/5 3/5) fractional order spots of the three $\sqrt{7} \times \sqrt{3}$ rotational domains are highlighted by yellow, blue, and red circles in LEED. An atomically resolved STM image of the $\sqrt{7} \times \sqrt{3}$-In phase is shown in the inset in (b). Dotted rectangle denotes the unit cell. (c)–(f) Kinematical simulations of the (00) CTR profile. Reciprocal lattice unit (r.l.u.) along the interface normal orientation is abbreviated as r.l.u. in the panels. (c) Two-ML-thick $\sqrt{7} \times \sqrt{3}$-In-rect film on the Si(111)$\sqrt{3} \times \sqrt{3}$-B substrate with Si adatoms. (d) Two-ML-thick $\sqrt{7} \times \sqrt{3}$-In-rect film on the Si(111)$\sqrt{3} \times \sqrt{3}$-B substrate without Si adatoms. (e) One-ML-thick $\sqrt{7} \times \sqrt{3}$-In-hex film on the Si(111)$\sqrt{3} \times \sqrt{3}$-B substrate with Si adatoms. (f) One-ML-thick $\sqrt{7} \times \sqrt{3}$-In-hex film on the Si(111)$\sqrt{3} \times \sqrt{3}$-B substrate without Si adatoms. The interlayer distances and R factor are indicated in each panel.

atoms on top of the subsurface B atoms [8,9,14–16]. In the simulation, Si and B atoms in the substrate were fixed at the coordinates of the Si(111)$\sqrt{3} \times \sqrt{3}$-B surface structural model which we had determined in a SXRD experiment [17]. The Si(111)7×7 surface reconstruction is also capped by Si adatoms at the top layer [18]. However, the interface missed Si adatoms and returned to the simple bulk-truncated Si(111)1×1 structure in the analysis of a previous SXRD study of the $\sqrt{7} \times \sqrt{3}$-In-rect on the Si(111)7×7 substrate [5]. Thus, we examined the one-ML-thick $\sqrt{7} \times \sqrt{3}$-In-hex and two-ML-thick rect structures on the Si(111)$\sqrt{3} \times \sqrt{3}$-B substrate with and without Si atoms in the simulation. The results of the simulations and the obtained interlayer distances are displayed with the R factor in Figs. 1(c)–1(f). The (00) CTR is sensitive to the stacking of layers along surface normal orientation. The experimentally observed (00) CTR profile

was satisfactorily reproduced by the two-ML-thick $\sqrt{7} \times \sqrt{3}$-In-rect film [Figs. 1(c) and 1(d)] but not by the one ML thick $\sqrt{7} \times \sqrt{3}$-In-hex film [Figs. 1(e) and 1(f)]. However, the presence or absence of the Si adatoms at the interface did not affect the quality of the fitting in the simulation. Our density functional theory (DFT) calculations revealed that the In layer was unstable unless the interface missed the Si adatoms. Thus, we consider that the two-ML-thick $\sqrt{7} \times \sqrt{3}$-In-rect film was formed on the Si adatom missing Si(111)$\sqrt{3} \times \sqrt{3}$-B substrate although the R factor in the missing adatom model was slightly larger than that with Si adatoms. The best fitting for the two-ML-thick $\sqrt{7} \times \sqrt{3}$-In-rect film on the Si adatom missing Si(111)$\sqrt{3} \times \sqrt{3}$-B interface is shown by a red solid curve in Fig. 1(d). The In-Si and In-In interlayer distances were deduced as 2.35 and 2.70 Å for the $\sqrt{7} \times \sqrt{3}$-In-rect film on the Si(111)$\sqrt{3} \times \sqrt{3}$-B substrate. In the meantime, the In-Si and In-In distances were reported to be 2.36 and 2.56 Å experimentally [5] and 2.40 and 2.58 Å theoretically [4] for the $\sqrt{7} \times \sqrt{3}$-In-rect film on the Si(111)7×7 substrate. The obtained interlayer distances are consistent with these values. The R factor was as small as 0.092 in the best fitting. Therefore, the two-ML-thick $\sqrt{7} \times \sqrt{3}$-In-rect film is considered to be formed successfully on the Si(111) $\sqrt{3} \times \sqrt{3}$-B substrate without Si adatoms.

B. Superconductivity

Scanning tunneling spectra (STS) revealed that the two-ML-thick $\sqrt{7} \times \sqrt{3}$-In film on the Si(111)$\sqrt{3} \times \sqrt{3}$-B substrate became superconductor at low temperature. A gap was observed to open at the Fermi level at temperatures of the STS device below 3 K in STS on the defect-free area [Fig. 2 (a)]. As expected for a superconductor, the gap was observed to be suppressed under magnetic field. Figure 2(b) displays the change of the gap by the application of external magnetic field B along the surface normal orientation. The gap reduced with the magnetic field and finally closed. It supports that the gap was caused by the superconductivity of the $\sqrt{7} \times \sqrt{3}$-In-rect film on the Si(111)$\sqrt{3} \times \sqrt{3}$-B substrate.

The size of the gap was evaluated by fitting the spectrum using the following equations which include the extended Bardeen-Cooper-Schrieffer (BCS) theory and the effect of temperature:

$$I(V) = \int_{\infty}^{-\infty} TN_t N_s(E)(f(E-V) - f(E))dE, \quad (1)$$

$$N_s(E) = \mathrm{Re}\left\{ \frac{|E| + i\Gamma}{\sqrt{(|E| + i\Gamma)^2 - \Delta^2}} \right\}. \quad (2)$$

Here, I, V, T, N_t, N_s, $f(E)$, Γ, Δ are the tunneling current, sample bias voltage, tunneling probability, density of states at tip and sample, Fermi distribution function at a temperature, quasiparticle lifetime broadening, and superconducting gap, respectively [19–22]. Γ, Δ, and T were taken as parameters for the fitting. An example of the fitting is shown in Fig. 2(c). We defined the temperature obtained by the fitting as the effective temperature. Δ, Γ, and the effective temperature were deduced by the fitting of the spectra shown in Fig. 2(a).

The effective temperatures and Δs estimated by the fitting are indicated by red circles in Fig. 2(d). Δ at 0 K was obtained as 0.34 meV, and T_c was deduced to be 2.38 K from the analysis of the temperature dependence of Δ using the BCS theory [23] [Fig. 2(b)]. Δ of 0.57 and 0.45 meV were reported for the $\sqrt{7} \times \sqrt{3}$-In film with a small number of defects on the Si(111)7×7 substrate [2,22]. However, the gap and T_c decreases near the defects [24]. T_c was reported to decrease from 3.3 to 2.9 and 2.3 K by the increase in the defect density from 1.8 to 5.7 and 8.5% for the $\sqrt{7} \times \sqrt{3}$-In-rect film on the Si(111)7×7 substrate in a recent study [25]. The defect density of our sample was ca. 10% on an average. In this respect, T_c of the $\sqrt{7} \times \sqrt{3}$-In film on the Si(111) $\sqrt{3} \times \sqrt{3}$-B substrate is considered to be almost the same as that on the Si(111)7×7 substrate.

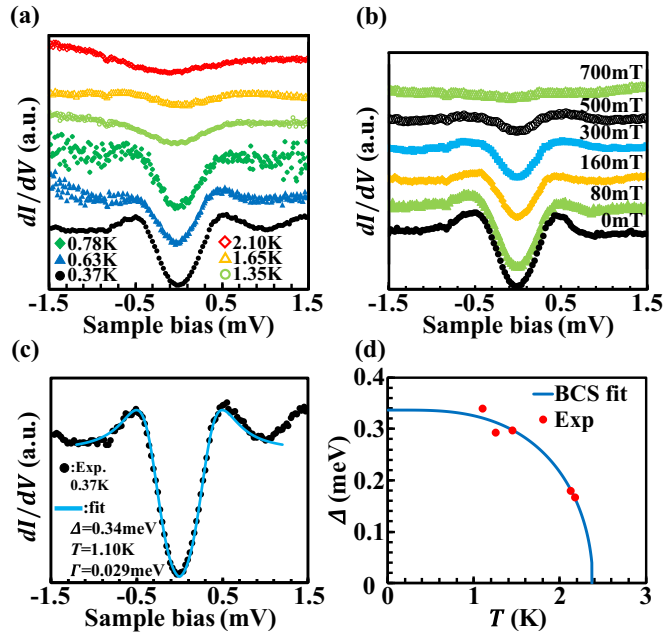

FIG. 2. (a) Temperature dependence of STS spectrum of the $\sqrt{7} \times \sqrt{3}$-In phase on the Si(111)$\sqrt{3} \times \sqrt{3}$-B substrate. The temperatures of the STS device are listed in the legend. (b) Suppression of the superconductivity gap in STS under magnetic fields. The spectra were taken at 0.63 K. (c) The fitting of the gap in STS at 0.37 K with Eqs. (1) and (2). The temperature of the STS device is 0.37 K and the effective temperature estimated by Dynes function is 1.10 K. (d) Temperature dependence of Δ and its BCS fitting. T_c was evaluated as 2.38 K. The effective temperatures and Δs estimated by fitting with the Dynes function are shown in the red circles.

C. Electronic structure

We investigated the electronic band structure of the $\sqrt{7} \times \sqrt{3}$-In film on the Si(111)$\sqrt{3} \times \sqrt{3}$-B substrate using ARPES at BL7U in Aichi SR. Samples were prepared *in situ* in an UHV apparatus. The reconstructions of the substrate and In film were observed using LEED. The Si(111)$\sqrt{3} \times \sqrt{3}$-B substrate was confirmed to be covered completely by the $\sqrt{7} \times \sqrt{3}$-In-rect film by observing the disappearance of the $\sqrt{3} \times \sqrt{3}$ diffraction spots. Although the Si(111)$\sqrt{3} \times \sqrt{3}$-B substrate was fully covered by the In film, a B core-level signal was observed. Considering together with the SXRD result, it evidenced that the B atoms at the subsurface site

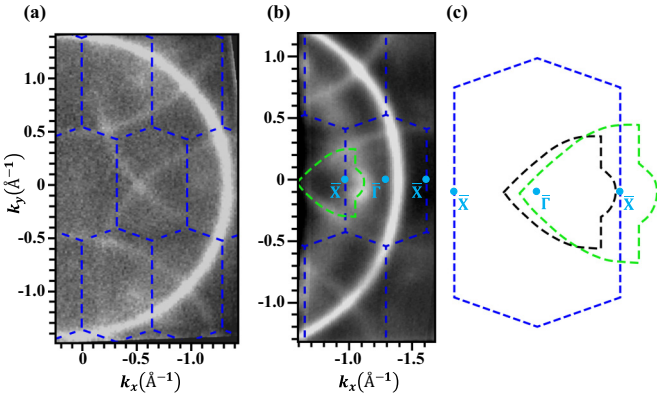

FIG. 3. The Fermi surface of the $\sqrt{7} \times \sqrt{3}$-In phase on the Si(111)$\sqrt{3} \times \sqrt{3}$-B substrate at $h\nu = 90$ eV (a) and 68 eV (b). The surface Brillouin zone of one of the three rotational domains of the $\sqrt{7} \times \sqrt{3}$-In phase is indicated by blue dashed lines in the figure. (c) An illustration of the butterfly-wing-shaped contour of the $\sqrt{7} \times \sqrt{3}$-In phase on the Si(111)$\sqrt{3} \times \sqrt{3}$-B (green dashed line) and Si(111)7×7 substrates (black dashed line) [26].

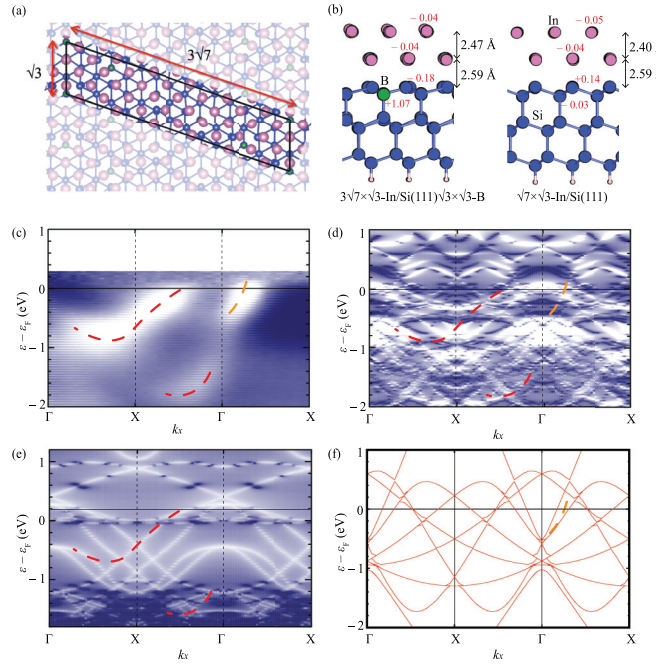

FIG. 4. (a) Top view for In/Si(111)$3\sqrt{7} \times \sqrt{3}$-B unit cell. Purple, blue, green spheres are In, Si, B atoms, respectively. (b) Optimized atomic structure of the two-ML-thick $\sqrt{7} \times \sqrt{3}$-In film on the Si(111)$\sqrt{3} \times \sqrt{3}$-B (left) and Si(111)1×1 (right) substrates. Interlayer distances and the number of transferred electrons at each atomic site are indicated in the figure. (c) A comparison of the experimentally observed and theoretically calculated band dispersions of the circular (orange dashed curve) and butterfly-wing-shaped (red dashed curve at the upper side) contours along the $\bar{\Gamma}$-$\bar{X}$-$\bar{\Gamma}$ direction at $h\nu = 68$ eV. (d) The calculated whole band dispersion of the two-ML-thick $\sqrt{7} \times \sqrt{3}$-In film on the Si-adatom-missing Si(111)$\sqrt{3} \times \sqrt{3}$-B substrate. (e) The calculated whole band dispersion of the Si-adatom-missing Si(111)$\sqrt{3} \times \sqrt{3}$-B substrate without In. The single-particle electron energy ε is relative to the calculated Fermi level ε_F. Note that computational and experimental Fermi levels do not coincide partly due to the doping effect. (f) The calculated band dispersion of freestanding In bilayer.

remained with the $\sqrt{3} \times \sqrt{3}$ periodicity as at the pristine Si(111)$\sqrt{3} \times \sqrt{3}$-B substrate surface although the Si adatoms were missing. ARPES measurements were conducted at room temperature.

The Fermi surface obtained by incident photon energies $h\nu$ of 90 eV and 68 eV are shown in Figs. 3(a) and 3(b), respectively. The circular Fermi contour of the two-dimensional free-electron-like band and its replicas with three rotational domains were clearly observed at the $\sqrt{7} \times \sqrt{3}$-In film on the Si(111)$\sqrt{3} \times \sqrt{3}$-B substrate as reported on Si(111)7×7 substrate [26]. The radius of the Fermi circle ($k_F = 1.40$ Å^{-1}) was the same as that on the Si(111)7×7 substrate. It clearly indicates that the nearly free-electron-like band is intrinsic to the $\sqrt{7} \times \sqrt{3}$-In film and emerges irrespective of the interface structure at the Si(111) substrate. In addition to the circular contours, other contours appeared in the areas enclosed by three circular arcs. The contours were observed more clearly at $h\nu = 68$ eV, as shown in Fig. 3(b). Since butterfly-wing-shaped contours were observed at the positions close to the present contours in the Fermi surface of the $\sqrt{7} \times \sqrt{3}$-In film on the Si(111)7×7 substrate [26], we call the contours butterfly-wing-shaped contours in this paper. However, the present butterfly-wing-shaped contours were slightly larger and shifted outward along the $\bar{\Gamma}$-$\bar{X}$ line than those on the Si(111)7×7 substrate as illustrated in Fig. 3(c). As shown in the energy dispersion in Fig. 4(c), the butterfly-wing band (the upper red dashed line) crossed the Fermi level at the point outside the second $\sqrt{7} \times \sqrt{3}$ Brillouin zone (BZ) (the left side $\bar{\Gamma}$-$\bar{X}$ zone in the figure) while it locates at the position almost touching the $\bar{X}$ point in the second BZ on the Si(111)7×7 substrate [4,26].

We conducted DFT calculations to elucidate the origin of the butterfly-wing-shaped contour of the two-ML-thick $\sqrt{7} \times \sqrt{3}$-In film on the Si(111)$\sqrt{3} \times \sqrt{3}$-B substrate. The generalized-gradient approximation parametrized by Perdew, Burke, and Ernzerhof for the exchange correlation functional [27] and the projector augmented-wave method [28,29] were employed as implemented in the VASP code [29]. The calculation was carried out for the $3\sqrt{7} \times \sqrt{3}$ unit cell in which both the unit cells of the $\sqrt{7} \times \sqrt{3}$-In and the Si(111)$\sqrt{3} \times \sqrt{3}$-B lattices become commensurate, as illustrated in Fig. 4(a). In calculations, 520 eV of cutoff energy and $5 \times 2 \times 1$ of **k** grid is adopted. Our slab model contains three bilayers of Si including one bottom bilayer, which is fixed to the geometry of bulk Si, saturated by H atoms. Each slab model is separated at least 10 Å of vacuum region along c axis. The calculated band dispersion of $3\sqrt{7} \times \sqrt{3}$ was unfolded to the first BZ of the $\sqrt{7} \times \sqrt{3}$-In film [30]. The layered structure of the two-ML-thick $\sqrt{7} \times \sqrt{3}$-In film was kept to be stable on the Si(111)$\sqrt{3} \times \sqrt{3}$-B substrate without Si adatoms as 30 meV/atom of In adsorption energy. However, the structure of In bilayer was completely hampered on the substrate with Si adatoms during the structural optimization, with relatively high In adsorption energy of 220 meV/atom. Thus, the calculation was carried out for the $\sqrt{7} \times \sqrt{3}$-In film

on the Si(111)$\sqrt{3} \times \sqrt{3}$-B substrate with the missing-adatom interface. The optimized structure of the $\sqrt{7} \times \sqrt{3}$-In film on the missing-adatom Si(111)$\sqrt{3} \times \sqrt{3}$-B and Si(111)1×1 substrates are illustrated in Fig. 4(b). The In-In and In-Si interlayer distances were 2.47 and 2.59 Å on the missing adatom Si(111)$\sqrt{3} \times \sqrt{3}$-B substrate. These values are consistent with those obtained in SXRD experiments (2.35 and 2.70 Å). The calculation also showed that the interlayer distances hardly change on the Si(111)1×1 substrate.

At the $\sqrt{3} \times \sqrt{3}$-B reconstruction, B atoms occupied the subsurface sites substitutionally [8,9,14,17]. Thus, the B site could draw electrons to dope holes to the $\sqrt{7} \times \sqrt{3}$-In film. However, Bader charge analysis [31] revealed that the electrons are donated to the subsurface B site from the surrounding Si atoms to leave the $\sqrt{7} \times \sqrt{3}$-In film free from the hole doping as indicated in Fig. 4(b). Thus, the shift of the butterfly-wing-shaped contour was not due to the shift of the Fermi level by the hole doping from the Si(111) $\sqrt{3} \times \sqrt{3}$-B substrate.

The experimentally observed band dispersion of the circular and butterfly-wing-shaped contours were reproduced by the DFT calculation as indicated by the orange and red dashed curves in Fig. 4(c). The whole band dispersion of the $\sqrt{7} \times \sqrt{3}$-In film on the missing-adatom Si(111)$\sqrt{3} \times \sqrt{3}$-B substrate is shown in Fig. 4(d). The band dispersion of the missing-adatom Si(111)$\sqrt{3} \times \sqrt{3}$-B substrate is represented in Fig. 4(e). The circular contour's band appeared in Figs. 4(d) and 4(f) but not in Fig. 4(e). In the meantime, the butterfly-wing-shaped contour's band appeared in Fig. 4(e). These mean clearly that the 2D free-electron-like circular contour is intrinsic of the $\sqrt{7} \times \sqrt{3}$-In film while the butterfly-wing-shaped contours originate from the Si substrate interface. Thus, the $\sqrt{7} \times \sqrt{3}$-In film on the Si(111)$\sqrt{3} \times \sqrt{3}$-B substrate is considered to emerge superconductivity similar to that on the Si(111)7×7 substrate irrespective of the difference in the substrate-mediated butterfly-wing-shaped contour band. In this respect, the interaction with the substrate is not thought to be crucial for the superconductivity of the two-ML-thick In film.

IV. SUMMARY

In summary, the $\sqrt{7} \times \sqrt{3}$-In-rect film was successfully synthesized on the Si(111)$\sqrt{3} \times \sqrt{3}$-B substrate. The film was confirmed to have the two-ML-thickness, while the interface preserved the $\sqrt{3} \times \sqrt{3}$-B reconstruction without Si adatoms by SXRD measurements. The two-ML-thick $\sqrt{7} \times \sqrt{3}$-In-rect film became a superconductor at $T_c = 2.38$ K on the Si(111)$\sqrt{3} \times \sqrt{3}$-B substrate. This T_c was recognized to be equivalent to that on the Si(111)7×7 substrate in previous reports with regard to the surface-defect density dependence of T_c.

The In film on the Si(111)$\sqrt{3}$-B substrate showed the two-dimensional free-electron-like circles and the butterfly-wing-shaped contour at the Fermi surface. The two-dimensional free-electron-like Fermi contour was identical to that on the Si(111)7×7 substrate. In the meantime, the butterfly-wing-shaped contour was shifted and enlarged on the $\sqrt{3}$-B substrate. The two-dimensional free-electron-like contour and butterfly-wing-shaped contour were revealed to originate from the In film and the Si substrate, respectively, by the DFT calculations. Thus, the superconductivity is not considered to be mediated by the interface.

ACKNOWLEDGMENTS

The synchrotron radiation experiments were performed at the BL13XU of SPring-8 with the approval of the Japan Synchrotron Radiation Research Institute (JASRI) (Proposal No. 2020A1139). This work was supported in part by KAKANHI (Grants in Aid for Scientific Research No. 9H00859). Low-temperature STM/STS measurements were carried out at the Institute for Solid State Physics, The University of Tokyo. We thank Dr. Yoshio Watanabe for providing us an opportunity to use the BL7U beamline of the Aichi Synchrotron Radiation Center. The DFT calculations were partly carried out by using supercomputers at ISSP, University of Tokyo, and TSUBAME, Tokyo Institute of Technology.

[1] S. Qin, J. Kim, Q. Niu, and C.-K. Shih, Science **324**, 1314 (2009).
[2] T. Zhang, P. Cheng, W.-J. Li, Y.-J. Sun, G. Wang, X.-G. Zhu, K. He, L. Wang, X. Ma, X. Chen, Y. Wang, Y. Liu, H.-Q. Lin, J.-F. Jia, and Q.-K. Xue, Nat. Phys. **6**, 104 (2010).
[3] T. Uchihashi, P. Mishra, M. Aono, and T. Nakayama, Phys. Rev. Lett. **107**, 207001 (2011).
[4] J. W. Park and M. H. Kang, Phys. Rev. Lett. **109**, 166102 (2012).
[5] T. Shirasawa, S. Yoshizawa, and T. Takahashi, and T. Uchihashi, Phys. Rev. B **99**, 100502(R) (2019).
[6] J.-F. Ge, Z.-L. Liu, C. Liu, C.-L. Gao, D. Qian, Q.-K. Xue, Y. Liu, and J.-F. Jia, Nat. Mater. **14**, 285 (2015).
[7] T. Ogino, V. M. Kuzumo, S. Yamazaki, K. Nakatsuji, and H. Hirayama, J. Phys.: Condens. Matter **32**, 415001 (2020).
[8] I.-W. Lyo, E. Kaxiras, and Ph. Avouris, Phys. Rev. Lett. **63**, 1261 (1989).
[9] E. Kaxiras, K. C. Pandey, F. J. Himpsel, and R. M. Tromp, Phys. Rev. B **41**, 1262 (1990).
[10] O. Sakata, Y. Furukawa, S. Goto, T. Mochizuki, T. Uruga, K. Takeshita, H. Ohashi, T. Ohata, T. Matsushita, S. Takahashi, H. Tajiri, T. Ishikawa, M. Nakamura, M. Ito, K. Sumitani, T. Takahashi, T. Shimura, A. Saito, and M. Takahashi, Surf. Rev. Lett. **10**, 543 (2003).
[11] H. Tajiri, H. Yamazaki, H. Ohashi, S. Goto, O. Sakata, and T. Ishikawa, J. Synchrotron Radiat. **26**, 750 (2019)
[12] J. Kraft, M. G. Ramsey, and F. P. Netzer, Phys. Rev. B **55**, 5384 (1997).
[13] Unpublished. The software is opened for beamline users.
[14] R. L. Headrick, I. K. Robinson, E. Vlieg, and L. C. Feldman, Phys. Rev. Lett. **63**, 1253 (1989).
[15] H. Huang, S. Y. Tong, J. Quinn, and F. Jona, Phys. Rev. B **41**, 3276 (1990).
[16] P. Baumgärtel, J. J. Paggel, M. Hasselblatt, K. Horn, V. Fernandez, O. Schaff, J. H. Weaver, A. M. Bradshaw, D. P.

Woodruff, E. Rotenberg, and J. Denlinger, Phys. Rev. B **59**, 13014 (1999).
[17] Y. Yoshiike, H. Tajiri, S. Yamazaki, K. Nakatsuji, and H. Hirayama, Jpn. J. Appl. Phys. **57**, 075701 (2018).
[18] K. Takayanagi, Y. Tanishiro, S. Takahashi, and M. Takahashi, Surf. Sci. **164**, 367 (1985).
[19] R. C. Dynes, V. Narayanamurti, and J. P. Garno, Phys. Rev. Lett. **41**, 1509 (1978).
[20] R. C. Dynes, J. P. Garno, G. B. Hertel, and T. P. Orlando, Phys. Rev. Lett. **53**, 2437 (1984).
[21] F. Herman and R. Hlubina, Phys. Rev. B **94**, 144508 (2016).
[22] S. Yoshizawa, H. Kim, T. Kawakami, Y. Nagai, T. Nakayama, X. Hu, Y. Hasegawa, T. Uchihashi, Phys. Rev. Lett. **113**, 247004 (2014).
[23] D. Guterding, S. Diehl, M. Altmeyer, T. Methfessel, U. Tutsch, H. Schubert, M. Lang, J. Müller, M. Huth, H. O. Jeschke, R. Valentí, M. Jourdan, and H.-J. Elmers, Phys. Rev. Lett. **116**, 237001 (2016).
[24] S. Yoshizawa, H. Kim, Y. Hasegawa, and T. Uchihashi, Phys. Rev. B **92**, 041410(R) (2015).
[25] M. Liu, H. Nam, J. Kim, G. A. Fiete, and C.-K. Shih, Phys. Rev. Lett. **127**, 127003 (2021).
[26] E. Rotenberg, H. Koh, K. Rossnagel, H. W. Yeom, J. Schäfer, B. Krenzer, M. P. Rocha, and S. D. Kevan, Phys. Rev. Lett. **91**, 246404 (2003).
[27] J. P. Perdew, K. Burke, and M. Ernzerhof, Phys. Rev. Lett. **77**, 3865 (1996).
[28] P. E. Blöchl, Phys. Rev. B **50**, 17953 (1994).
[29] G. Kresse and J. Furthmüller, Phys. Rev. B **54**, 11169 (1996).
[30] V. Wang, N. Xu, J. C. Liu, G. Tang, and W. T. Geng, Comput. Phys. Commun. **267**, 108033 (2021).
[31] G. Henkelman, A. Arnaldsson, and H. Jónsson, Comput. Mater. Sci. **36**, 354 (2006).